Monte Carlo transient phonon transport in silicon and germanium at nanoscales

David Lacroix,* Karl Joulain,† and Denis Lemonnier‡
Laboratoire d'Études Thermiques, ENSMA, 1, Avenue Clément Ader 86960 Futuroscope Cedex, France
(Received 8 April 2005; revised manuscript received 6 July 2005; published 23 August 2005)

Heat transport at nanoscales in semiconductors is investigated with a statistical method. The Boltzmann transport equation (BTE), which characterizes phonon motion and interaction within the crystal lattice, has been simulated with a Monte Carlo technique. Our model takes into account media frequency properties through the dispersion curves for longitudinal and transverse acoustic branches. The BTE collisional term involving phonon scattering processes is simulated with the relaxation times approximation theory. A new distribution function accounting for the collisional processes has been developed in order to respect energy conservation during phonons scattering events. This nondeterministic approach provides satisfactory results in what concerns phonon transport in both ballistic and diffusion regimes. The simulation code has been tested with silicon and germanium thin films; temperature propagation within samples is presented and compared to analytical solutions (in the diffusion regime). The two-material bulk thermal conductivity is retrieved for temperature ranging between 100 K and 500 K. Heat transfer within a plane wall with a large thermal gradient (250 K to 500 K) is proposed in order to expose the model ability to simulate conductivity thermal dependence on heat exchange at nanoscales. Finally, size effects and validity of heat conduction law are investigated for several slab thicknesses.

DOI: 10.1103/PhysRevB.72.064305 PACS number(s): 63.20.−e, 05.10.Ln, 44.10.+i, 65.40.−b

I. INTRODUCTION

The development of nanotechnologies has led to an unprecedented size reduction of the electronic and mechanical devices. For example, transistors of a few nanometer size are now openly considered.[1] The heat that will be dissipated by joule effect in these semiconductor junctions will reach soon the levels of the heat dissipated in a light bulb. This high volumetric heat dissipation in electronic devices will have to be evacuated very efficiently in order to avoid possible failures of the systems. This task will not be achieved without a precise knowledge of the phenomena governing the heat transfer at nanoscale. Furthermore, new technologies based on a local heating are being developed in order to enlarge the computer hard disk capacity. The ultimate limit of storage is to write a byte at the atomic scale. This goal is already feasible with near-field microscope probes but at a too slow rate. A way to write bytes at the nanometer scale is the melting of a polymer by heating it on a very short time scale ($\leqslant$1 ns) by an array of heated near-field probes.[2] In this example, the heat transfer has to be controlled not only at the nanometer scale but also at the nanosecond scale.

Through these two examples, one can anticipate that the foreseeing technological challenges in miniaturization will have to solve more and more problems of heat transfer at short time and space scale. However, the physics of heat transfer usually used (Fourier's law, radiative transfer equation) can no longer be applied when some characteristic length scales are reached.[3] In thermal radiation, for example, wave effects appear as the system characteristic lengths becomes lower than the typical wavelength ($\lambda \sim 10\ \mu$m at $T = 300$ K).[4,5] A substantial increase of the radiative heat transfer can even be reached at nanometric distances.[6] On its side, heat conduction is classically described by the Fourier law and the heat conduction equation ($\partial T/\partial t = \alpha \Delta T$) which is a diffusion equation. It is well known that this kind of equation can be interpreted as a random walk of particles.[7] In the case of heat conduction, we are actually dealing with energy carriers which are electrons in metals and phonons in crystalline materials. When these carriers undergo a large number of collisions, the use of the diffusion equation is valid whereas a more careful study is required when the number of interactions between carriers lowers.

A way to achieve this goal is to consider the evolution of a distribution function $f(\mathbf{r},\mathbf{p},t)$ which describes the number of particles in a certain elementary volume $d^3\mathbf{r}d^3\mathbf{p}$ around the point $(\mathbf{r},\mathbf{p})$ in the phase space. The evolution equation of f, called the Boltzmann transport equation (BTE), makes f vary in space and time under the influence of advection, external force, and collision.[8] Note that this approach is not relevant to treat the wave aspects of the problem such as interference or tunneling. The understanding and the modeling of the collision term is actually the key point in the resolution of the BTE. It can sometimes be fully expressed as in radiation transfer. Then the collision term is in that case the sum of an absorption term, an elastic scattering term, and an emission term proportional to an equilibrium distribution.[9] Many resolution techniques have been developed in radiation transfer such as the discrete ordinates method, the Monte Carlo method, or the ray-tracing method.[10] They can hardly be used when the collision processes are inelastic as it is the case for electrons and phonons.[11] For example, the phonons, which are eigenmodes of the harmonic oscillators constituting the crystal, can only interact through the anharmonic term of the potential leading to three or more phonon collisions. These interactions preserve neither the number of phonons nor their frequency in the collision process. Nevertheless, these three or four phonon interactions tend to restore thermal equilibrium, i.e., to help the phonons to follow an equilibrium distribution func-

tion which can be easily determined from thermodynamic equilibrium considerations. Thus, many of the studies approximate the collision term in the BTE by the so-called relaxation time approximation: the distribution function $f(\mathbf{r},\mathbf{p},t)$ relaxes to an equilibrium function $f^0(\mathbf{r},\mathbf{p})$ on a time scale $\tau(\mathbf{p})$. The BTE resulting from this approximation is nothing but the radiative transfer equation without scattering.[12] All the numerical tools developed in thermal radiation can therefore be used in this case. The key point in this model is to calculate a suitable $\tau(\mathbf{p})$ in order to characterize the collisions.

In the middle of the 20th century, a great theoretical effort has been made to determine the relaxation times of the phonons in a bulk material. At ambient temperature, it has been shown that the main contribution to the relaxation time finds its origin in the anharmonic phonon interaction. These anharmonic interactions can be triadic or quartic. Triadic interactions involve three phonons (for example, two phonons anihilate to give birth to a third one) whereas quartic interactions involve four phonons (two phonon anihilate to give birth to two others). Quartic interactions contribute often less to the phonon relaxation time, but sometimes have to be taken into account, especially in the case of high temperatures ($T>1000$ K) as it has been shown by Ecsedy and Klemens.[13] At ambient and low temperature, semiconductor (such as Si and Ge, which are treated here) studies are usually limited to triadic interactions.[14] Nevertheless, taking them into account or not does not change the ways the BTE can be solved. Among these anharmonic processes, two different kinds can be identified. The so-called normal processes (N), which maintain the momentum in the collision, and the Umklapp processes (U), which do not preserve the momentum. The former do not affect the material thermal resistance, contrary to the latter. These Umklapp processes follow selection rules[15] and it is an amazing feat to calculate them.[16]

In the case of semiconductors such as silicon (Si), germanium (Ge),[17,18] and gallium arsenide (GaAs),[19,20] the relaxation times have allowed us to compute semianalytically thermal conductivities in good agreement with measurements. Resolution of the BTE have been achieved on these materials in bulk situations, thin film, or superlattice configuration.[12,21–23] At short time scale, these resolutions have been compared to classical solutions[24,25] and some modifications of the BTE have been proposed.[26] The resolutions based on the discrete ordinates method or on the finite volumes method converge very quickly numerically but have a major drawback: they are governed by a single relaxation time taking into account all the different processes of relaxation such as the anharmonic interactions between phonons, the interactions with impurities and dislocations, or the scattering on the material boundaries. The Matthiesen rule, which states that the inverse of the total relaxation term is the sum of the relaxation times due to every different phenomena, is usually used. In the context of the BTE in the relaxation time approximation, this means that all the different interaction or scattering phenomena tend to restore thermal equilibrium.

An alternative way to solve the BTE is the Monte Carlo method. This method is quite computer time greedy because it necessitates to following a large number of energy carriers, but it becomes competitive when the complexity of the problem increases, particularly for nontrivial geometries. This method is therefore useful in order to calculate the heat transfer in electronic devices of any shape. Moreover, in this method, different scattering phenomena (impurities scattering, boundary scattering, and inelastic scattering) can be treated separately. The resolution of the BTE by the Monte Carlo method has been performed for electrons[27–32] but has been little used in the case of phonons. Peterson[33] performed a Monte Carlo simulation for phonons in the Debye approximation with a single relaxation time. He presented results both in the transient regime and in equilibrium situation. Mazumder and Majumdar[34] followed Peterson's approach but included in their simulation the dispersion and the different acoustic polarization branches. They retrieved both the ballistic and the diffusion situation but did not show any result in the transient regime. Another limit of this last paper is that the N processes and the U processes are not treated separately although they do not contribute in the same way to the conductivity.

The starting point in our work is these two contributions. We follow individual phonons in a space divided into cells. The phonons, after a drift phase, are able to interact and to be scattered. The speed and the rate at which phonons scatter depends on the frequency. We ensure that energy is conserved after each scattering process. This procedure is different whether the phonons interact through an N process or a U process. This paper is therefore an improvement of existing phonon Monte Carlo methods and is validated on simple examples such as a semiconductor film heated at two different temperatures.

Section II recalls the basic hypothesis governing the BTE. Fundamental quantities such as the number of phonons, the energy, and the density of states are also defined. The phonon properties are also presented through their dispersion relations. Section III exposes the Monte Carlo method used in this paper. Boundary conditions, phonon drift, and scattering procedures are given in detail. Section IV presents transient results in the diffusion and ballistic regimes. Thermal conductivities of silicon and germanium between 100 K and 500 K are numerically estimated. The influence of conductivity thermal dependence on heat conduction within a slab is studied. Finally, size effects on phonon transport at very short scales are considered.

II. THEORY

A. Boltzmann transport equation

The Boltzmann transport equation (BTE) is used to model the phonon behavior in a crystal lattice. This equation is related to the variation of the distribution function $f(t,\mathbf{r},\mathbf{K})$ which depends on time t, location $\mathbf{r}$, and wave vector $\mathbf{K}$. $f(t,\mathbf{r},\mathbf{K})$ can also be defined as the mean particle number at time t in the $d^3\mathbf{r}$ volume around $\mathbf{r}$ with $\mathbf{K}$ wave vector and $d^3\mathbf{K}$ accuracy. In the absence of external force, the BTE expression is[35]

$$\frac{\partial f}{\partial t}+\nabla_{\mathbf{K}}\omega\cdot\nabla_{\mathbf{r}}f=\left.\frac{\partial f}{\partial t}\right|_{\text{collision}} \tag{1}$$

with the phonon group velocity $\mathbf{v}_g=\nabla_{\mathbf{K}}\omega$.

Integration of the distribution function over all the wave vectors of the first Brillouin zone and all the locations leads to the phonon number $N(t)$ at a given time in the crystal. The lhs term of Eq. (1) accounts for the phonon drift in the medium and the rhs term for the equilibrium restoration due to phonon collisions with themselves, impurities, and boundaries.

The collisional term modeling is the key point in the BTE resolution. In the case of photons, it appears as the sum of an absorption term, of an emission term, and of an elastic scattering term in which a scattering phase function relates a photon in the incoming and outgoing propagation directions during a scattering event.[9] However, in the case of phonons, there is no absorption, nor emission, but only scattering events. Scattering events at the borders can simply be treated during the drift phase, i.e., when a phonon reaches a border. Scattering with impurities can be treated similarly to the isotropic scattering of photons when addressing thermal radiation. Scattering of phonons due to the anharmonic terms of the potential are quite difficult to express. We know nevertheless that these terms are responsible for the thermal conductivity, i.e., tend to restore thermal equilibrium. Therefore, in this work we use the relaxation time approximation for three phonon scattering processes. The collision time used in this formalism comes from normal and Umklapp relaxation times which are further estimated.

B. Lattice modeling

As it has been exposed previously, the thermal behavior of the crystal can be considered from the phonon characteristics (location, velocity, and polarization) within the medium. They might be obtained through the BTE solution since the distribution function can be easily related to the energy and therefore to the temperature. Using an integrated distribution function, one can express the total vibrational energy of the crystal as[36]

$$E = \sum_{p} \sum_{\mathbf{K}} \left(\langle n_{\mathbf{K},p} \rangle + \frac{1}{2} \right) \hbar \omega, \tag{2}$$

where $\langle n_{\mathbf{K},p} \rangle$ is the local thermodynamic phonon population with polarization p and wave vector $\mathbf{K}$ described by the Bose-Einstein distribution function

$$\langle n_{\mathbf{K},p} \rangle = \frac{1}{\exp\left(\frac{\hbar \omega}{k_B T} \right) - 1}. \tag{3}$$

E is the material volumic energy. It is obtained by summation in Eq. (2) of each quantum $\hbar\omega$ over the two polarizations for transverse, longitudinal, and optical modes of phonon propagation. Assuming that the phonon wave vectors are sufficiently dense in the $\mathbf{K}$ space, the summation over $\mathbf{K}$ can be replaced by an integral. Moreover, using $D_p(\omega)$, the phonon density of state, we can achieve the integration in the frequency domain. This two modifications yield

$$E = \sum_{p} \int_{\omega} \left(\langle n_{\omega,p} \rangle + \frac{1}{2} \right) \hbar \omega D_p(\omega) g_p d\omega, \tag{4}$$

with $D_p(\omega)d\omega$ the number of vibrational modes in the frequency range $[\omega, \omega + d\omega]$ for polarization p and g_p the degeneracy of the considered branch. In the case of an isotropic three-dimensional crystal ($V = L^3$) we have[36]

$$D_p(\omega) d\omega = \frac{d\mathbf{K}}{(2\pi/L)^3} = \frac{V K^2 dK}{2\pi^2}. \tag{5}$$

The $1/2$ term in Eq. (2) is the constant zero point energy which does not participate to the energy transfer in the material, therefore it has been suppressed. Using the group velocity definition, Eq. (4) might be rewritten

$$E = V \sum_{p} \int_{\omega} \left[\frac{\hbar \omega}{\exp\left(\frac{\hbar \omega}{k_B T} \right) - 1} \right] \frac{K^2}{2\pi^2 v_g} g_p d\omega. \tag{6}$$

The numerical scheme we are going to present is mainly based upon energy considerations. The previous expression Eq. (6) will be also used to estimate the material temperature by means of a numerical inversion.

C. Dispersion curves

Only a few studies on that topic take into account dispersion. Indeed, frequency dependence makes calculations longer, accounting for velocity variation. However, realistic simulation of phonon propagation through the crystal must take into account interaction between the different branches. Here optical phonons are not considered because of their low group velocity: they do not contribute significantly to the heat transfer. These modes can actually contribute indirectly through the interaction with other modes such as the acoustic modes. By modifying their relaxation times, they can inflence the total thermal conductivity of the material. Nevertheless, in this work, we did not consider this phenomenon. Consequently only transverse and longitudinal branches of silicon and germanium are presented here (Fig. 1). We have made the common isotropic assumption for wave vectors and consider the [001] direction in $\mathbf{K}$ space. For silicon, we used data obtained from a quadratic fit,[31] whereas germanium experimental curves[37] have been fitted by cubic splines. Phonon group velocity has then been extracted from this data. Note that in silicon and germanium, two acoustic branches have been considered. The transverse branch is degenerated ($g_T = 2$) whereas the longitudinal branch is non-degenerated ($g_L = 1$).

III. MONTE CARLO METHOD

The Monte Carlo technique has been widely used in order to solve transport equations. In the heat transfer field, Monte Carlo solutions of radiative transfer equation are often considered as reference benchmarks. The method accuracy only lies on the number of samples used. Among others, the main advantages of this method are

- the simple treatment of transient problems,

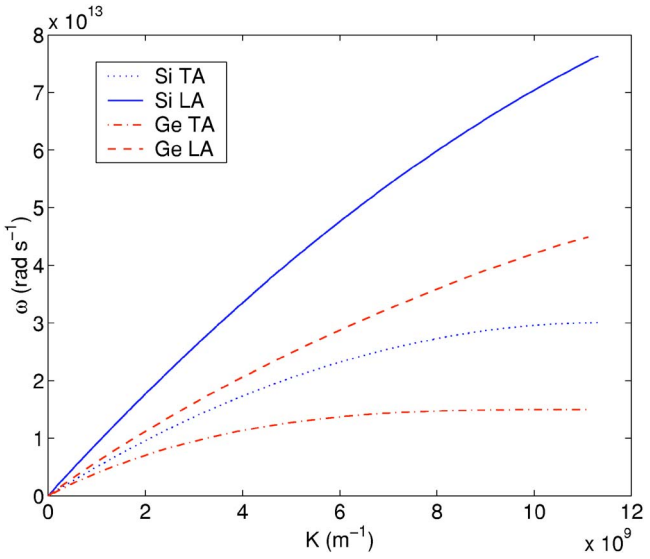

FIG. 1. (Color online) Phonon dispersion curves for silicon and germanium in the first Brillouin zone, $\mathbf{K}_{\max\,\mathrm{Si}}=1.1326\times10^{10}$ m^{-1} and $\mathbf{K}_{\max\,\mathrm{Ge}}=1.1105\times10^{10}$ m^{-1}.

- the ability to consider complex geometries, and
- the possibility to follow independently each scattering process (for instance, phonon-phonon, phonon-impurity, and phonon-boundary processes).

The main drawback is computational time. However, this method remains a good choice between deterministic approaches such as the discrete ordinates method (DOM) or "exact solutions" such as those provided by molecular dynamics which is limited to very small structures.

A. Simulation domain and boundary conditions

As it was said before, the geometry of the studied material does not matter. Here, a simple cubic cells stack (Fig. 2) is considered since it can be readily related to the plane wall geometry commonly used in thermal problems. Cylindrical cells or multidimensional stacks can also be considered in order to model nanowires or real semi-conductors.

Concerning boundary conditions, we assume that the lateral walls of the cells (in x and y directions) are specularly reflecting in most of the simulation cases. This means that walls are adiabatic and perfectly smooth. Note also that in that case, the dimension in the x and y directions should not change the result in the simulation. Indeed, when reflection is specular on the lateral cells boundaries, the momentum is preserved in the z direction. The heat flux and the temperature along z should thus not be affected. At both ends of the medium, temperature is assumed to be constant. Therefore, energy in the first and the last cells is calculated from equilibrium distribution functions. Incoming phonons in these cells are thermalized at each time step. Consequently theses cells act as blackbodies.

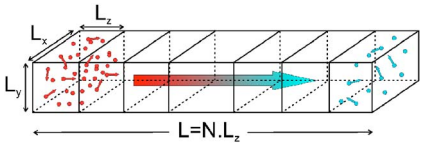

FIG. 2. (Color online) Studied model. Phonon location, energy, and velocity are randomly chosen in each cell according to dispersion curves and local temperature.

At this stage, an important point is the choice of the three discretizations: temporal, spatial, and spectral. Spatial discretization is directly related to the material geometry: usually cells length are about $L_z\sim100$ nm for micrometric objects and can be smaller in the case of thin films or nanowires, for instance. The time step choice depends on two parameters: the cell size and the group velocity at a given frequency. In order to consider all scattering events and to avoid ballistic jump over several cells, we state that the time step must be lower than $\Delta t<L_z/V_g^{\max}$.

The spectral discretization is uniform; we used $N_b=1000$ spectral bins in the range $[0,\omega_{\mathrm{LA}}^{\max}]$. We have checked that larger discretizations do not increase the result accuracy.

B. Initialization

The first step of the simulation procedure, once medium, geometry, and mesh have been chosen, is to initialize the state of phonons within each cell describing the material. Hence, the number of phonons present in each cell is required. It will be obtained considering the local temperature within the cell and using a modified expression of Eq. (6). In this equation, energy is given for all the quanta $\hbar\omega$ associated to a spectral bin. Therefore, it can be rewritten to give the total number of phonons in a cell as

$$N=V\sum_{p=\mathrm{TA,LA}}\sum_{b=1}^{N_b}\left[\frac{1}{\exp\left(\frac{\hbar\omega_{b,p}}{k_BT}\right)-1}\right]\frac{K_{b,p}^2}{2\pi^2v_{gb,p}}g_p\Delta\omega. \quad (7)$$

The number of phonons obtained with Eq. (7) is usually very large, for instance in a 10 nm silicon cube at 300 K, N can be estimated around 5.45×10^5. In the case of nanoscale structures, direct simulations can be achieved if the temperature is relatively low. In the case of microscale samples or multidimensional cell stacking, a weighting factor shall be used to achieve Monte Carlo simulations. Hence, Peterson's[33] technique has been used. The actual number of phonons N is divided by a constant weight W in order to obtain the number of simulated phonons $N^\star$

$$N^\star=\frac{N}{W}. \quad (8)$$

In our simulations W's value is set around $W\sim10^4$ for micrometric structures, in order to preserve accuracy.

During the initialization process, a temperature step is prescribed in the medium. The first cell is raised to the hot temperature T_h, the last to the cold one T_c. All the phonons in the intermediate boxes are also at T_c. Associated theoretical energy in the whole structure is obtained from Eq. (6). This energy should match the calculated energy $E^\star$ within all the cells, written into the following form:

$$E^{\star} = \sum_{c=1}^{N_{\text{cell}}} \sum_{n=1}^{N^{\star}} W \times \hbar \omega_{n,c}. \tag{9}$$

As a consequence, during the initialization, phonons should be added by packs of W at a given frequency, sampled from a normalized number density function F. According to Mazumder and Majumdar's work,[34] this function is constructed doing the cumulative summation of the number of phonons in the ith spectral bin over the total number of phonons Eq. (7):

$$F_i(T) = \frac{\sum_{j=1}^{i} N_j(T)}{\sum_{j=1}^{N_b} N_j(T)}. \tag{10}$$

In this process, a random number R is drawn (all the random numbers discussed here check $0 \leqslant R \leqslant 1$) and the corresponding value F_i gives the frequency ω_i, knowing that the $F_{i-1} \leqslant R \leqslant F_i$ location is achieved with a bisection algorithm. The actual frequency of the phonon is randomly chosen in the spectral interval prescribing

$$\omega_i = \omega_{0,i} + (2R - 1)\frac{\Delta\omega}{2}, \tag{11}$$

where $\omega_{0,i}$ is the central frequency of the ith interval.

Once the frequency is known, the polarization of the phonon has to be determined. It can belong to the TA or LA branch with respect to the Bose-Einstein distribution and the density of states. For a given frequency ω_i, the number of phonons on each branch are $N_{\text{LA}}(\omega_i) = \langle n_{\text{LA}}(\omega_i) \rangle D_{\text{LA}}(\omega_i)$ and $N_{\text{TA}}(\omega_i) = 2 \times \langle n_{\text{TA}}(\omega_i) \rangle D_{\text{TA}}(\omega_i)$, where the density of states are calculated with Eq. (5) in which the relation between ω and K are taken from the dispersion curves. The associated probability to find a LA phonon is expressed as

$$P_{\text{LA}}(\omega_i) = \frac{N_{\text{LA}}(\omega_i)}{N_{\text{LA}}(\omega_i) + N_{\text{TA}}(\omega_i)}. \tag{12}$$

A new random number R is drawn: if $R < P_{\text{LA}}(\omega_i)$, the phonon belongs to the LA branch, otherwise it is a transverse one.

The knowledge of the frequency and the polarization leads to the estimation of the phonon group velocity and the phonon wave vector merely using the dispersion curves and their derivatives. Assuming isotropy within the crystal, the direction $\mathbf{\Omega}$ is obtained from two random numbers R and R' randomly distributed between 0 and 1. Indeed, chosing a direction in 3D consists in chosing two angles (θ, ϕ) which are the spherical coordinates angles. Moreover, these angles have to be chosen so that the corresponding directions are uniformly distributed in the 4π full space solid angle. The elementary solid angle is $d\Omega = \sin\theta d\theta d\phi = -d(\cos\theta)d\phi$ so we see that $\cos\theta$ has to be uniformly distributed between -1 and 1 and ϕ beteween 0 and 2π. Hence $\mathbf{\Omega}$ is written as

$$\mathbf{\Omega} = \begin{cases} \sin\theta\cos\phi \\ \sin\theta\sin\phi \\ \cos\theta \end{cases} \tag{13}$$

where $\cos\theta = 2R - 1$ and $\phi = 2\pi R'$.

The last operation of the initialization procedure is to give a random position to the phonon within the cell. In the grid previously considered, location of the nth phonon in the cell c, whose lengths are L_x, L_y, and L_z, is

$$\mathbf{r}_{\text{n,c}} = \mathbf{r}_{\text{c}} + L_x R\mathbf{i} + L_y R'\mathbf{j} + L_z R''\mathbf{k} \tag{14}$$

where $\mathbf{r}_{\text{c}}$ is the coordinates of the cell and R, R', and R'' are three random numbers.

C. Drift

Once the initialization stage is achieved, phonons are allowed to drift inside the nanostructure. Considering the time step Δt and their velocities, each phonon position is updated: $\mathbf{r}_{\text{drift}} = \mathbf{r}_{\text{old}} + \mathbf{v}_{\text{g}}\Delta t$. In the case of shifting outside of the lateral boundaries (in $\mathbf{i}$ and $\mathbf{j}$ directions), the phonon is specularly reflected at the wall. In the case of diffuse reflection with a particular degree d ($0 \leqslant d \leqslant 1$, $d=0$ purely specular, $d=1$ purely diffuse) a random number R is drawn. When R is lower than d a new phonon propagation direction is calculated using Eq. (13).

When a phonon reaches the bottom (z_{min}) or the top (z_{max}) of a cell, it is allowed to carry on its way in the previous or next cell, respectively. As a result, it is going to modify the cell energy and by extension its local temperature. At the end of the drift phase, the actual energy $\widetilde{E^{\star}}$ is computed in all the cells using Eq. (9). Then, the actual temperature $\tilde{T}$ is obtained with Eq. (6) doing a Newton-Raphson inversion.[38] Phonons drifting in the first and last boxes are thermalized to the cold or hot temperature in order to keep boundary cells acting as blackbody sources.

D. Scattering

In the Monte Carlo simulation, the scattering process has been treated independently from the drift. The phonon-phonon scattering aims at restoring local thermal equilibrium in the crystal since it changes phonon frequency. Collisions with impurities or crystal defects as well as boundary scattering do not change frequency but solely the direction $\mathbf{\Omega}$. These last phenomena are significant when low temperatures are reached and the phonon mean free path becomes large. In the present study we do not consider impurity and defect scattering for calculation. Besides, the bulk hypothesis is assumed, there is no boundary scattering. The phonons are specularly reflected at the side limits. Hence, only three-phonon interactions have been considered.

As already said before, there are two kinds of three-phonon processes: normal processes (N) which preserve momentum and Umklapp processes (U) which do not preserve momentum by a reciprocal lattice vector. These two mechanisms have consequences on the thermal conductivity of the crystal. When the temperature is sufficiently high ($T \gtrsim T_{\text{Debye}}$), U processes become significant and directly

modify heat propagation due to the resistivity effect on energy transport. On the other hand, normal scattering also affects heat transfer since it modifies frequency distribution of the phonons. For phonons described by $(p,\omega,\mathbf{K})$ and $(p',\omega',\mathbf{K}')$ scattering to $(p'',\omega'',\mathbf{K}'')$, the following relations are checked

$$\text{energy:} \quad \hbar\omega + \hbar\omega' \leftrightarrow \hbar\omega'',$$

$$N \text{ processes:} \quad \mathbf{K} + \mathbf{K}' \leftrightarrow \mathbf{K}'',$$

$$U \text{ processes:} \quad \mathbf{K} + \mathbf{K}' \leftrightarrow \mathbf{K}'' + \mathbf{G}, \tag{15}$$

where $\mathbf{G}$ is a lattice reciprocal vector. Scattering also involves polarization in the way that acoustic transverse and longitudinal phonons can interact. According to Srivastava,[39] for N and U processes different combinations are possible:

N and U processes:

$$\mathrm{T} + \mathrm{T} \rightleftharpoons \mathrm{L}, \quad \mathrm{L} + \mathrm{T} \rightleftharpoons \mathrm{L}, \text{ and } \mathrm{T} + \mathrm{L} \rightleftharpoons \mathrm{L},$$

$$N \text{ processes only:} \quad \mathrm{T} + \mathrm{T} \rightleftharpoons \mathrm{T} \text{ and } \mathrm{L} + \mathrm{L} \rightleftharpoons \mathrm{L}. \tag{16}$$

For the N processes only, all the participating phonons must be collinear to achieve scattering. Usually these interactions are neglected.

Direct simulation of phonons scattering is an awkward challenge. With Monte Carlo simulations, it is possible to estimate phonon collisions with neighbors as in the gas kinetic theory calculating a three-particle interaction cross section. However, in the present study, the frequency discretization might not be sufficiently thin to assess every three-phonon processes. Thus the collisional process is treated in the relaxation time approximation. Several studies on that topic have been carried out since the early work of Klemens;[15] a detailed paper of Han and Klemens[14] recalled them.

Relaxation times τ have been proposed for several crystals. They depend on the scattering processes, the temperature, and the frequency. Holland's work on silicon[18] and the recent study of Singh for germanium[40] provide various τ values. The independence of the scattering processes is used to consider a global three-phonon inverse relaxation time accounting for N and U processes τ_{NU}. It has been obtained using the Mathiessen rule $(\tau_{NU}^{-1} = \tau_N^{-1} + \tau_U^{-1})$.

In order to be implemented in the Monte Carlo simulation, the scattering routine requires an associated collision probability P_{scat}. This one is derived saying that the probability for a phonon to be scattered between t and $t+dt$ is dt/τ. Thus,

$$P_{\text{scat}} = 1 - \exp\left(\frac{-\Delta t}{\tau_{NU}}\right). \tag{17}$$

A random number R is drawn; if $R < P_{\text{scat}}$, the phonon is scattered. As a result, new frequency, polarization, wave vector, group velocity, and direction have to be resampled with respect of energy and momentum conservation. Relaxation times are temperature and frequency dependent. For each simulated phonon considered τ_{NU} is calculated at every time step.

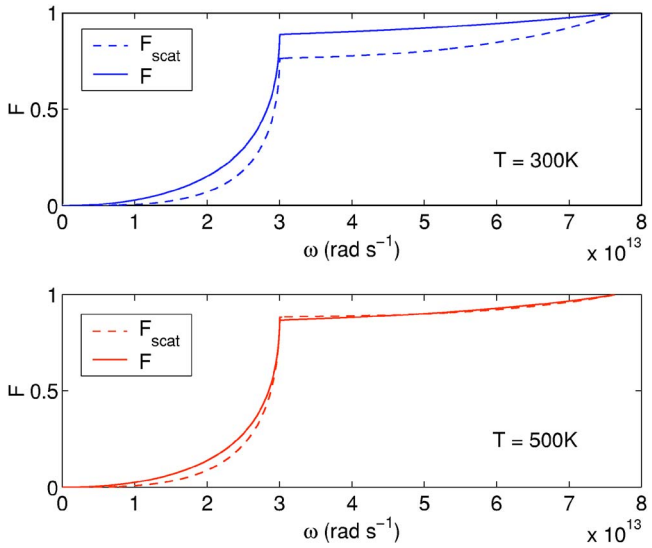

FIG. 3. (Color online) Normalized number density function in silicon with and without P_{scat} correction.

In previous studies on that topic,[33,34] the frequency sampling after collision was achieved from the normalized number density function F at the actual temperature $\tilde{T}$ of the cell obtained at the end of the drift procedure. In this approach the actual energy after the scattering stage is usually different from the "target" one obtained with temperature $\tilde{T}$. Hence a subsequent "creation/destruction" scheme is necessary to ensure energy conservation. In fact, in the preceding procedure at thermal equilibrium, the probability of destroying a phonon of frequency ω and polarization p is different from the probability of creating this phonon. This means that the Kirchhoff law (creation balances destruction) is not respected. In order to create phonons at the same rate they are destroyed at thermal equilibrium, the distribution function used to sample the frequencies of the phonons after scattering has to be modulated by the probability of scatterring. So we define a new distribution function

$$F_{\text{scat}}(\tilde{T}) = \frac{\sum_{j=1}^{i} N_j(\tilde{T}) \times P_{\text{scat } j}}{\sum_{j=1}^{N_b} N_j(\tilde{T}) \times P_{\text{scat } j}}. \tag{18}$$

Taking into account the scattering probability in the distribution function F_{scat} ensures that a destructed phonon on both transverse and longitudinal branches can be resampled with a not too weak energy as it can be seen in Fig. 3.

According to the described simulation procedure after the initialization step, phonons in cell c are described by $[T_c, F(T_c), N^{\star}(T_c), E^{\star}(T_c)]$. They are allowed to drift and the state of cell c before scattering is $[\tilde{T}_c, F(T_c), N'^{\star}(\tilde{T}_c), E'^{\star}(\tilde{T}_c)]$. Then three-phonons collisions occur and change energy by frequency resetting of the colliding phonons (using the distribution function F_{scat}, leading to the final state $[\tilde{T}_c,\ F_{\text{scat}}(\tilde{T}_c),\ N'^{\star}(\tilde{T}_c),\ E''^{\star}(\tilde{T}_c)]$). Hence energy can be expressed as

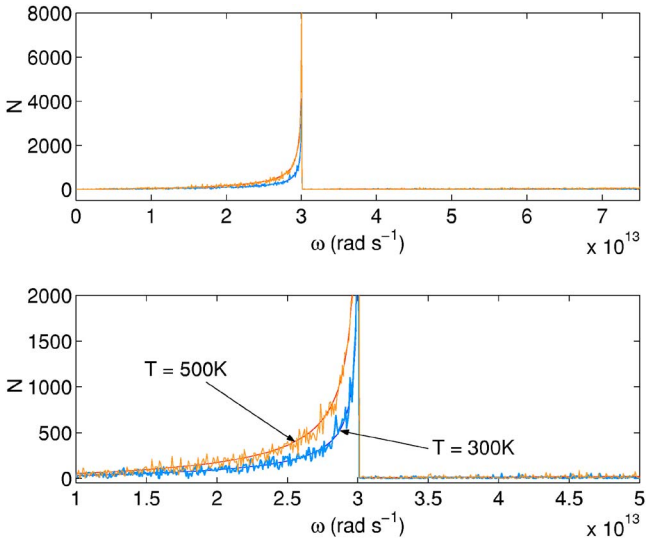

FIG. 4. (Color online) Frequency spectra at 300 K and 500 K for silicon.

$$E''^{\star} = \underbrace{\sum_{i=1}^{N'^{\star}_{\mathrm{scat}}} \hbar\tilde{\omega}i}_{\Rightarrow F_{\mathrm{scat}}(\tilde{T}_c)} + \underbrace{\sum_{i=1}^{N'^{\star}-N'^{\star}_{\mathrm{scat}}} \hbar\omega_i}_{\Rightarrow F(T_c)} \tag{19}$$

Furthermore the number of colliding phonons can simply be expressed as $N'^{\star}_{\mathrm{scat}}(\tilde{T}_c)=P_{\mathrm{scat}}\times N'^{\star}(\tilde{T}_c)$. One then sees that, if we want to preserve energy at thermal equilibrium, the new normalized number density function F_{scat} must take into account this collisional probability. Energy conservation during Monte Carlo simulation might be noticed from frequency distribution (Fig. 4, which matches the theoretical distribution given by Eq. (7)].

Concerning momentum conservation, the task is harder to address since the Monte Carlo process considers phonons one by one. Consequently triadic N or U interactions cannot be rigorously treated. In a first approach, we propose the following procedure to take into account the fact that U processes contribute to the thermal resistance whereas the N processes do not. When the phonons scatter through a U process, their directions after scattering are randomly chosen as in the initialization procedure. Therefore, these phonons are randomly scattered and contribute to the diffusion of heat. On the contrary, it is assumed that scattering phonons experiencing an N process do not change their propagation direction $\mathbf{\Omega}$.

Statistically, for a given temperature and frequency, the phonons are destroyed by scattering at the same rate they appear. A phonon which scatters has a great chance to be replaced in the computation by a phonon of a near frequency. Therefore, by this treatment, the N processes "approximately" preserve momentum. Nevertheless, a more accurate treatment should be done in order to respect exactly the momentum in the N processes. For a plane-parallel geometry, it seems possible to guarantee the momentum conservation in a single direction.

In fact, the relaxation time estimation[14] states that there is a frequency limit ω_{limit} for the transverse acoustic branch. ω_{limit} actually corresponds to $\mathbf{K}=\mathbf{K}_{\mathrm{max}}/2$. Below this limit frequency, there are no U processes. On the other hand, for $\omega>\omega_{\mathrm{limit}}$, N processes are no longer considered and the propagation direction must be resampled in the case of a collision. In what concerns the longitudinal acoustic branch, there is no limit frequency. According to Holland[18] only N processes exist. However, applying this assumption implies that momentum has to be conserved for each scattering event involving a LA phonon. This leads to thermal conductivity values higher than the theoretical ones for temperatures between 100 K and 250 K. In order to ensure a more realistic momentum conservation we set that half of the colliding phonons keep their original $\mathbf{\Omega}$, and the others (U processes) are directionally resampled.

IV. RESULTS AND DISCUSSION

Different kinds of simulations have been performed so as to check the computational method. Tests in both diffusion and ballistic regimes are carried out for silicon and germanium. Moreover, if small thermal gradients are considered, one can estimate the thermal conductivity k from the heat flux through the structure. This has been realized for Si and Ge between 100 K and 500 K.

Knowing that the conductivity varies with temperature according to a power law in the case of Si and Ge for T greater than 100 K, it is obvious that a large thermal gradient applied to our media should not bring a purely linear solution. Hence simulations in this specific case have been done. We will see that our model correctly predicts the steady-state regime when compared to the steady-state analytical solution.

Eventually, we studied size effects on thermal behavior of nanostructures. It appears that the ballistic regime can be retrieved at room temperature when the sample size is close to the nanometer scale.

A. High-temperature transient calculations

Concerning high-temperature transient calculations, the simulated case is described by the following parameters:

- hot and cold temperatures: $T_h=310$ K and $T_c=290$ K,
- medium geometry: stack of 40 cellules ($L_x=L_y=5\times10^{-7}$ m,$L_z=5\times10^{-8}$ m),
- time step and spectral discretization: $\Delta t=5$ ps and $N_b=1000$ bins, and
- weighting factor: $W=3.5\times10^4$ for Si and $W=8\times10^4$ for Ge.

Both materials were tested. Germanium calculation results are presented here (Fig. 5). In order to assess the Monte Carlo solution, transient theoretical comparison exists in the case of the Fourier limit. Nevertheless, it requires that the thermal diffusivity α remains constant. In the chosen temperature range, according to the IOFFE database,[41] Ge thermal diffusivity is equal to $\alpha=0.36\times10^{-4}$ m^2 s^{-1}.

The considered test case has been described in Özişik's book[42] on the heat conduction equation. Within the described structure heat transfer is along the z axis and analytical so-

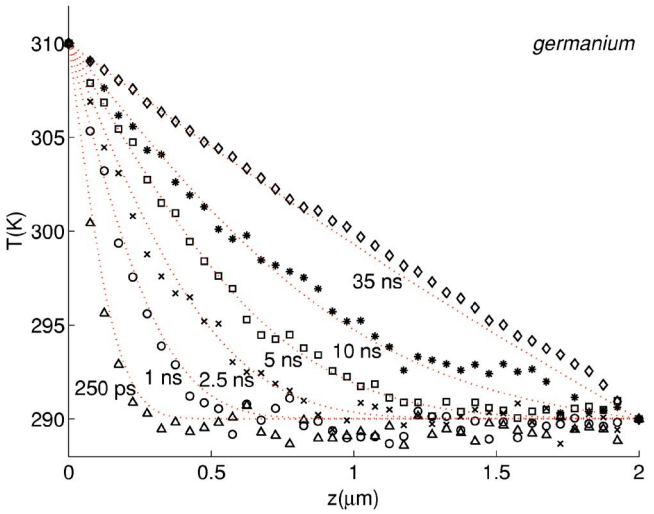

FIG. 5. Transient temperature in Fourier's regime for germanium and comparison with the analytical solution of heat conduction equation with a constant thermal diffusivity ($\alpha_{Ge}=0.36\times10^{-4}$ m^2 s^{-1}) (dotted curves).

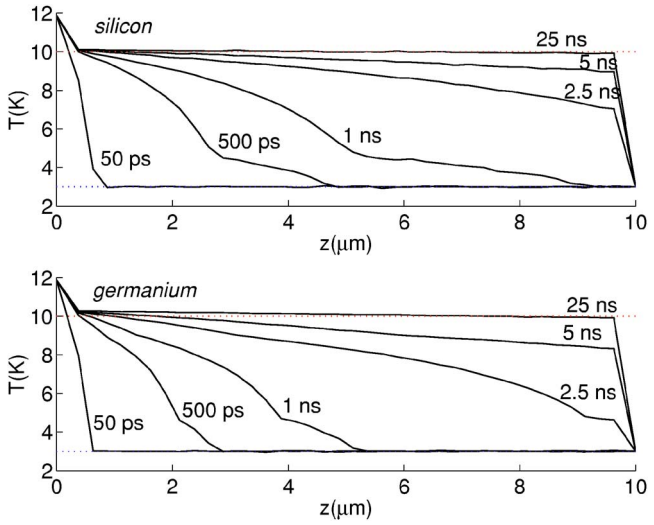

FIG. 6. (Color online) Transient temperature in the ballistic regime for silicon and germanium.

lution for a one-dimensional medium could be obtained from an integral transform. Temperature distribution in the slab is given by an infinite sum that requires enough terms in the case of short time calculation. However, a simpler analytical solution might be obtained with Laplace's transform

$$\frac{T(z,t)-T(L,t)}{T(0,t)-T(L,t)}=\left[\operatorname{erfc}\left(\frac{z}{2\sqrt{\alpha t}}\right)-\operatorname{erfc}\left(\frac{2L-z}{2\sqrt{\alpha t}}\right)+\operatorname{erfc}\left(\frac{2L+z}{2\sqrt{\alpha t}}\right)\right], \tag{20}$$

with erfc the complementary error function. The theoretical solution is only valid for short time and its accuracy is better than 1% if the Fourier number (Fo$=\alpha t/L^2$) checks Fo$\leqslant$0.7. In the case of a 2 μm germanium slab it leads to $t\leqslant$78 ns, which is large enough to reach steady state.

The calculated values have been obtained from ten simulations being averaged (Fig. 5), the random number seed being reset for each computations. The Monte Carlo model's ability to predict correctly temperature from the first moments till steady state is clearly illustrated. The remaining noise can be reduced with lower values of W weighting factor. The diffusion regime is obtained after 30 ns. Similar results are obtained for silicon, however the simulated slab has to be larger ($L=4$ μm) because ballistic effects are observed near the cold limit. This point will be discussed later.

B. Low-temperature transient calculations

For low temperatures, heat transport inside the slab is different since phonon interactions change. In this case U collisions are negligible and the only resistive processes are assigned to impurities, defects, and boundary scattering. These phenomena have to be carefully assessed in the case of thermal conductivity estimation below 100 K. In fact, for very low temperatures the phonon mean free path grows and becomes larger than the structure length. Hence, phonons can travel from hot to cold extremities without colliding. This is the ballistic regime similar to the one observed with photons exchanged between two black plates at different temperatures.[43] In this peculiar case temperature in steady state is equal to the following constant value:

$$T_{\text{ballistic}}=\left[\frac{T_h^4+T_c^4}{2}\right]^{1/4} \tag{21}$$

The simulation case parameters are

- hot and cold temperatures: $T_h=11.88$ K, $T_c=3$ K, and $T_{\text{ballistic}}=10$ K;
- medium geometry: stack of 40 cellules ($L_x=L_y=5\times10^{-7}$ m,$L_z=2.5\times10^{-7}$ m);
- time step and spectral discretization: $\Delta t=5$ ps and $N_b=1000$ bins; and
- weighting factor: $W=20$ for Si and $W=30$ for Ge.

Results for silicon and germanium (Fig. 6) give the expected results for the ballistic limit. It can be noticed that the current representation exhibits an artificial link between black boundaries and the first medium cell due to the spatial discretization.

It can be seen that hot phonons do not fly straight toward the cold limit. More than 1 ns is necessary to heat the last cell in the case of silicon. This is in agreement with velocities prescribed by dispersion curves. Heat propagation in germanium is slower since phonon group speed is also lower. Note also that in both materials, the temperature seems to propagate at two different velocities. For example, the 500 ps and 1 ns temperature curves exhibit two components. The fastest one propagates at the longitudinal wave velocity whereas the slowest is traveling at the transverse wave velocity. Results at low temperatures obtained with our method have already been predicted by Joshi and Majumdar[24] in similar cases, who applied successfully the equation of phonon radiative transfer (EPRT) in the ballistic regime.

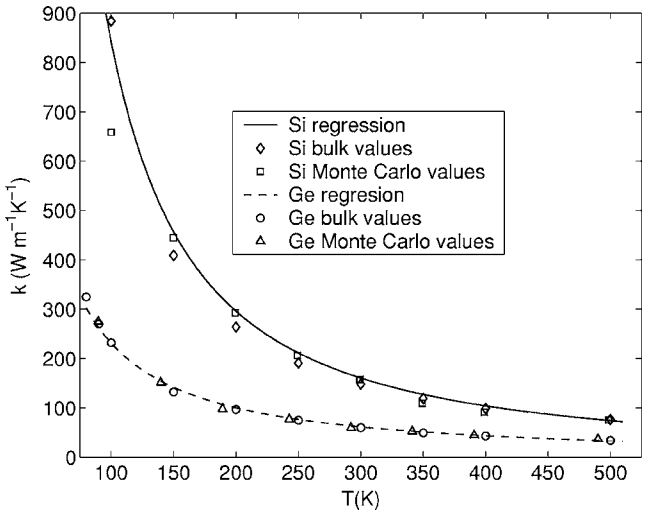

FIG. 7. Silicon and germanium thermal conductivities; comparison between bulk theoretical values and Monte Carlo calculated values.

C. Si and Ge thermal conductivities

There are several ways to perform the thermal conductivity calculation of a semiconductor. Among these techniques, Holland's method[18] based on phonons kinetic theory was largely employed. Molecular dynamic simulations can also be used to obtain k. In the present study thermal conductivity has been determined knowing the heat flux (phonon energy transport) through the medium for a given thermal gradient directly applying Fourier's law. As in Mazumder's work,[34] the temperature difference between hot and cold extremities is set to 20 K so as to determine average conductivities. The phonon heat flux is calculated along the z axis according to the following relation:

$$\phi = \sum_{n=1}^{N^\star} W\hbar\omega_n \mathbf{v}_{\mathrm{gn}} \cdot \mathbf{k}. \tag{22}$$

Simulations have been carried out between 100 K and 500 K (Fig. 7) on 2 μm thick samples.

Comparison of the Monte Carlo calculated conductivities is achieved with bulk data. Solid and dashed curves are linear power law regression of theoretical data in the considered thermal range. These values are used in next analytical calculations. We have appraised for 200 K$\leqslant T \leqslant$600 K;

$$k_{\mathrm{Si}}(T) = \frac{\exp(12.570)}{T^{1.326}},$$

$$k_{\mathrm{Ge}}(T) = \frac{\exp(10.659)}{T^{1.150}}. \tag{23}$$

For germanium a very good agreement is obtained with bulk values in the whole temperature domain. The maximum relative error is under 8%. In this case, at 100 K, the phonon mean free path is lowered to the micrometer according to Dames.[44] Consequently the stucture size is large enough to assume the acoustic thick limit. Furthermore, this calculation benefits from recent relaxation time estimation, which has been fixed with a good accuracy.[40] The influence of these factors on calculated conductivity is usually strong. Silicon results are also close to the bulk ones until 150 K where the relative error is equal to 7%. For lower temperatures, discrepancy between theory and simulation increases. This gap can be assigned to size effects since the phonon mean free path grows when temperature is falling. Here, it becomes similar to the slab size. Yet, if we refer to Asheghi's[45] work on thin films, thermal conductivity, at temperatures below 100 K, significantly decreases in comparison with bulk property due to stronger reduction of phonon mean free path by boundaries. Actually, for pure 3 μm silicon film, thermal conductivity is close to 600 W m^{-1} K^{-1} at 100 K.[45] This value is comparable to the 658 W m^{-1} K^{-1} obtained for our 2 μm film by Monte Carlo simulation.

D. Effect of nonlinear conductivity

In this fourth part, transient simulations with samples heated under a large thermal step have been conducted. The purpose of such calculations was to underline the model capacity to correctly predict steady state when medium properties $[k(T)]$ vary with temperature. In the previous part thermal conductivities of both bulk materials have been estimated with a power law [Eq. (23)]. Hence, the analytic solution for temperature profile within a slab can be easily determined in steady state by the resolution of a first-order differential equation as

$$T(z)_{\text{Steady state}} = \left[\left(\frac{z}{L}\right) T_c^{(\gamma+1)} + \left(1 - \frac{z}{L}\right) T_h^{(\gamma+1)} \right]^{1/(\gamma+1)}, \tag{24}$$

where conductivity can be written as $\lambda(T) = C \times T^{\gamma}$.

In order to avoid boundary effects in the case of silicon, a 4 μm thick sample, with larger cells ($L_z = 1 \times 10^{-7}$ m), is used. The initial geometry is kept for the germanium slab. Temperatures are now $T_h = 500$ K and $T_c = 250$ K. The time step remains equal to 5 ps. In both cases (Fig. 8) Monte Carlo simulations give a very good estimation of the steady-state behavior. Results are averaged over five computations on the last 1000 time steps (i.e., after 45 ns of elapsed time). At the cold limit of the germanium sample a weak deviation exists between simulation and theory. The relative error on temperature remains smaller than 1.5%, in this area. This mismatch could be assigned to boundary effects, associating diffusive and ballistic regimes near the limits as we will detail in the last part. It could also be due to the accuracy of the bulk thermal conductivity fitting at low temperatures.

Besides, inversion of such curves can theoretically provide the variation of k on a given thermal range, as long as the medium is in the acoustic thick limit.

E. Size effect on heat diffusion

From the previous calculations, it is obvious that the phonon mean free path modification with the temperature acts as a major factor in heat conduction. So, if the structure size is adjusted in order to match the mean free path at any temperature, ballistic phenomena should be observed. In this

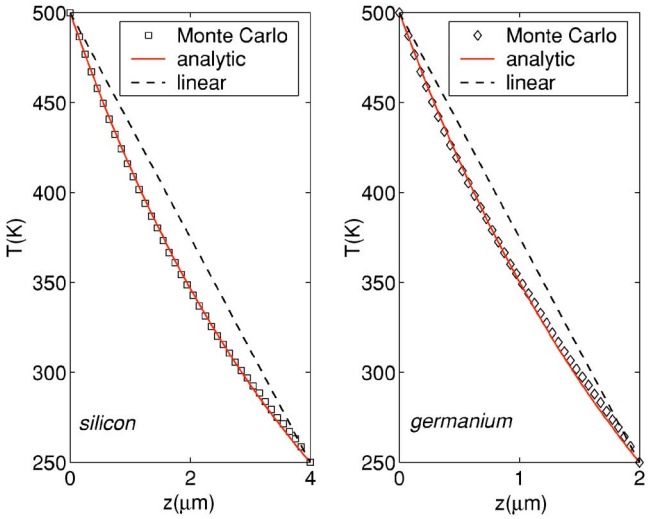

FIG. 8. (Color online) Steady-state temperature in Fourier's regime for silicon and germanium in the case of a large thermal gradient; comparison to the heat conduction equation analytical solution for temperature dependent conductivity.

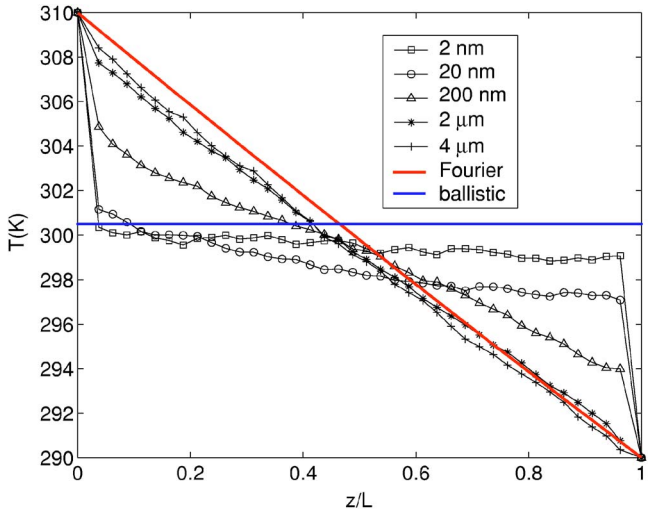

FIG. 9. (Color online) Steady-state temperature for silicon, influence of the slab thickness; comparison to the analytical solution in the diffusive and ballistic limits.

study only silicon is used and the simulation parameters are

- hot and cold temperatures: $T_h=310$ K and $T_c=290$ K,
- number of cells: 40, and
- total length and time step $(L,\Delta t)$: (2 nm, 5×10^{-3} ps), (20 nm, 5×10^{-2} ps), (200 nm, 5×10^{-1} ps), (2μm, 5 ps), and (4μm, 5 ps).

Weighting parameters and lateral cell lengths are adjusted in order to keep approximately 18 000 phonons in each cell.

Temperature profiles when steady state is reached have been plotted for each sample versus adimensional length z/L. Comparison to diffusive and ballistic regime is displayed in Fig. 9. With the imposed boundary temperatures the ballistic limit is equal to $T_{\text{ballistic}}=300.5$ K.

In the case of structure length lower than 200 nm ballistic trend mixed to phonon diffuse transport is observed. The temperature profile gets closer to the ballistic limit for sample size around the nanometer scale. Nevertheless, this approximately represents ten atom layers and therefore might encounter the simulation limitation. On the contrary, in a silicon sample thicker than 4 μm, temperature reaches the Fourier's regime and can be similarly obtained with heat conduction equation at least cost.

V. CONCLUSIONS

An improved Monte Carlo scheme that allows transient heat transfer calculations at time and space nanoscales, on the basis of phonon transport, has been presented. This model accounts for phonon transitions between longitudinal and transverse acoustic branches and can be simply applied to several semiconductors if their dispersion relations are known. A particular attention has been paid to the energy and momentum conservation during collision process.

Numerical result forecasts have been successfully assessed in different heat transfer modes. In slab configuration, a good agreement was found for both extreme phonon motions which are the diffusive and ballistic ones. Bulk thermal conductivities of silicon and germanium have been numerically retrieved with a maximal error lower than 8%. Besides, our Monte Carlo model correctly predicts temperature profile in more peculiar situations, when strong thermal gradient or very small sizes are encountered.

Nevertheless some key points need to be refined. Among them the momentum conservation procedure might be improved, especially for one-dimensional applications. Also, a treatment of the optical phonons influence would improve our model. Indeed, according to the recent study of Narumanchi,[25] capacitive properties prediction need the optical phonons to be taken into account. This influence seems less critical for conductivity predictions in the studied temperature range.[13] Moreover, regarding the collision process, improvements might be expected. Using theoretical values of τ recalled by Han and Klemens,[14] direct calculation of phonon scattering relaxation time can be realized in each authorized spectral bin. Hence, a more realistic approach of three-phonon interactions should be achieved.

We are currently working on these improvements but also on other potential implementations of the method such as those related to the superlattices and the nanowires.

*Also at Laboratoire d'Énergétique et de Mécanique Théorique et Appliquée, Université Henri Poincaré, Nancy 1, 54506 Vandœuvre Cedex, France. Electronic address: David.Lacroix@lemta.uhp-nancy.fr
†Electronic address: karl.joulain@let.ensma.fr
‡Electronic address: denis.lemonnier@let.ensma.fr

[1] *International Technology Roadmap for Semiconductors*, URL http://public.itrs.net.
[2] P. Vettiger, G. Gross, M. Despont, U. Dreschler, U. Dürig, B. Gotsmann, W. Häberle, M. Lantz, H. Rothuizen, R. Stutz, and G. Binnig, IEEE Trans. Nanotechnol. **1**, 39 (2001).
[3] D. Cahill, W. Ford, K. Goodson, G. Mahan, A. Majumdar, H. Maris, R. Merlin, and S. Phillpot, J. Appl. Phys. **93**, 793 (2003).
[4] D. Polder and D. V. Hove, Phys. Rev. B **4**, 3303 (1971).
[5] J. J. Loomis and H. J. Maris, Phys. Rev. B **50**, 18517 (1994).
[6] J. Mulet, K. Joulain, R. Carminati, and J.-J. Greffet, Appl. Phys. Lett. **78**, 2931 (2001).
[7] A. Einstein, Ann. Phys. **17**, 549 (1905).
[8] J. Ziman, *Electrons and Phonons* (Oxford University Press, Oxford, 1960).
[9] S. Chandrasekhar, *Radiative Transfer* (Dover, New York, 1960).
[10] M. Modest, *Radiative Heat Transfer* (Academic Press, San Diego, 2003), 2nd ed.
[11] L. Landau and E. Lifshitz, *Physical kinetics: volume 10 (Course of theoretical physics)* (Pergamon Press, Oxford, 1981).
[12] A. Majumdar, J. Heat Transfer **115**, 7 (1993).
[13] D. Ecsedy and P. Klemens, Phys. Rev. B **15**, 5957 (1977).
[14] Y.-J. Han and P. G. Klemens, Phys. Rev. B **48**, 6033 (1993).
[15] P. Klemens, Proc. R. Soc. London, Ser. A **208**, 108 (1951).
[16] C. Herring, Phys. Rev. **95**, 954 (1954).
[17] J. Callaway, Phys. Rev. **113**, 1046 (1959).
[18] M. Holland, Phys. Rev. **132**, 2461 (1963).
[19] J. Waugh and G. Dolling, Phys. Rev. B **4**, 3303 (1971).
[20] C. Bhandari and G. Verma, Phys. Rev. **140**, A2101 (1965).
[21] G. Chen, J. Heat Transfer **119**, 220 (1997).
[22] K. Goodson, J. Heat Transfer **118**, 279 (1996).
[23] D. Lemonnier and M. Lallemand, Heat Technol. **18**, 63 (2000).
[24] A. Joshi and A. Majumdar, J. Appl. Phys. **74**, 31 (1993).
[25] S. Narumanchi, J. Heat Transfer **126**, 946 (2004).
[26] G. Chen, Phys. Rev. Lett. **86**, 2297 (2001).
[27] C. Jacobini and L. Reggiani, Rev. Mod. Phys. **55**, 645 (1983).
[28] M. V. Fischetti and S. E. Laux, Phys. Rev. B **38**, 9721 (1988).
[29] P. Lugli, P. Bordone, L. Reggiani, M. Rieger, P. Kocevar, and S. M. Goodnick, Phys. Rev. B **39**, 7852 (1989).
[30] M. V. Fischetti and S. E. Laux, Phys. Rev. B **48**, 2244 (1993).
[31] E. Pop, R. Dutton, and K. Goodson, J. Appl. Phys. **96**, 4998 (2004).
[32] E. Pop, R. Dutton, and K. Goodson, Appl. Phys. Lett. **86**, 082101 (2005).
[33] R. Peterson, J. Heat Transfer **116**, 815 (1994).
[34] S. Mazumder and A. Majumdar, J. Heat Transfer **123**, 749 (2001).
[35] N. Ashcroft and N. Mermin, *Solid State Physics* (Saunders College, Philiadelphia, 1976), international ed.
[36] C. Kittel, *Introduction to Solid State Physics* (John Wiley and Sons, Philadelphia, 2004).
[37] G. Nilson and G. Nelin, Phys. Rev. B **3**, 364 (1971).
[38] W. Press, B. Flannery, S. Teukolsky, and W. Vetterling, *Numerical Recipes, The Art of Scientific Computing* (Cambridge University Press, Cambridge, 1960).
[39] G. Srivastava, *The Physics of Phonons* (Adam Hilger, Bristol, UK, 1990).
[40] B. Singh, M. Roy, V. Menon, and K. Sood, J. Phys. Chem. Solids **64**, 2369 (2003).
[41] *Semiconductors on nsm*, URL http://www.ioffe.rssi.ru/SVA/NSM/Semicond/.
[42] M. N. Özişik, *Boundary Value Problems of Heat Conduction* (Dover Publications, New York, 1968).
[43] M. Heaslet and R. Warming, Int. J. Heat Mass Transfer **8**, 979 (1965).
[44] C. Dames and G. Chen, J. Appl. Phys. **89**, 682 (2003).
[45] M. Asheghi, K. Kurabayashi, R. Kasnavi, and K. Goodson, J. Appl. Phys. **91**, 5079 (2002).